

Gyro Evaluation for the Mission to Jupiter

Sergei A. Jerebets
 Jet Propulsion Laboratory
 California Institute of Technology
 4800 Oak Grove Drive
 Pasadena, CA 91109
 jerebets@jpl.nasa.gov

Abstract—As an important component in NASA’s New Frontiers Program, the Jupiter Polar Orbiter (Juno) mission is designed to investigate in-depth physical properties of Jupiter. It will include the giant planet’s ice-rock core and atmospheric studies as well as exploration of its polar magnetosphere. It will also provide the opportunity to understand the origin of the Jovian magnetic field.

Due to severe radiation environment of the Jovian system, this mission inherently presents a significant technical challenge to Attitude Control System (ACS) design since the ACS sensors must survive and function properly to reliably maneuver the spacecraft throughout the mission.

Different gyro technologies and their critical performance characteristics are discussed, compared and evaluated to facilitate a choice of appropriate gyro-based inertial measurement unit to operate in a harsh Jovian environment to assure mission success.^{1,2}

gyros and star trackers would be used for the primary [1] mode with the gyros propagating attitude based on sensed rate between star measurements.

Based on their functionality, three basic types [2] of those sensors – rate gyros (RG), rate-integrating gyros (RIG) and control moment gyros (CMG) – are commonly employed to control and guide a spacecraft. As attitude sensors, RG measure spacecraft angular rates and RIG – angular displacements, correspondingly, about some initial reference. CMG are used to generate attitude control torques in response to a given command.

Gyros importance is found on their ability to provide an autonomous and continuous output [3] without a need of external reference, unlike in case of a star tracker.

TABLE OF CONTENTS

1. INTRODUCTION.....	1
2. MECHANICAL GYROS.....	2
3. OPTICAL GYROS.....	3
4. MEMS GYROS	4
5. GYRO PERFORMANCE CHARACTERISTICS.....	4
6. HRG	7
7. GYRO VENDORS	8
8. SUMMARY	8
REFERENCES	8
BIOGRAPHY	9

1. INTRODUCTION

To efficiently operate a spacecraft, the ACS processor will compute the vehicle current attitude, compare it with the desired one, and then determine and communicate the torques required to adjust the difference. As a typical combination (Fig. 1) of inertial and rate sensors, ACS will employ star trackers, sun sensors and gyros.

Being a valuable part of ACS, gyros are used to sense angular motion in conventional strap-down inertial systems. For low accuracy attitude acquisition and safe-hold mode a combination of gyros and sun sensors might suffice. The

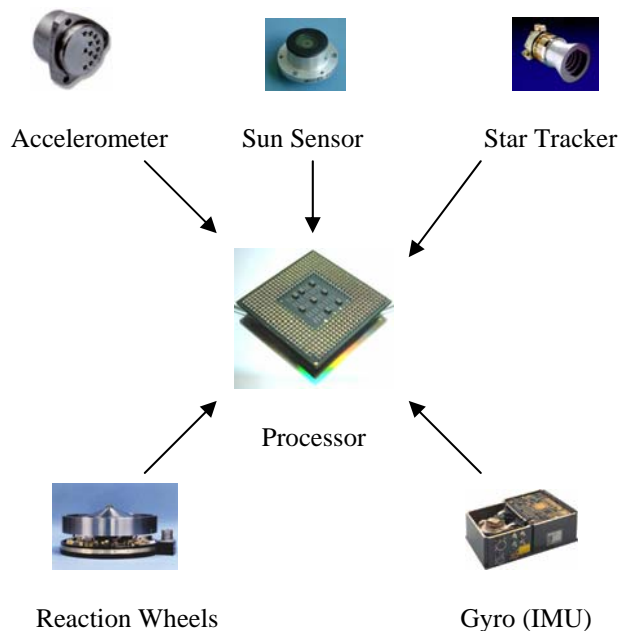


Figure 1 – ACS integration and realization.

Based on their construction, varieties of gyro types can be referenced by three gyro classes as mechanical, optical or MEMS, microelectromechanical systems.

¹ 1-4244-0525-4/07/\$20.00 ©2007 IEEE.

² IEEEAC paper #1642, Version 4, Updated December 1, 2006

2. MECHANICAL GYROS

Traditional mechanical gyro class (Figs. 2 and 3) includes single-degree-of-freedom (SDF) and two-degree-of-freedom (TDF) gyros.

The inertial element (rotor) of SDF gyro has its spin axis (SA) restrained to rotate (Fig. 2) about a single axis or output axis (OA). The reference axis is body fixed and coincident with the gyro SA at null.

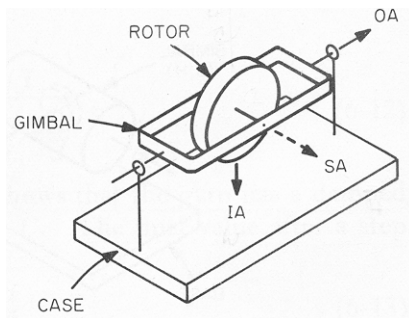


Figure 2 – SDF gyro schematics (after [4]).

The gyro sensitive axis – the input axis (IA) – is also body fixed and is perpendicular to the reference axis and OA. The gyro application is based on a utilizing the angular momentum, L conservation theorem from physics which can be read as $T = L \times \omega$ (Fig.2)

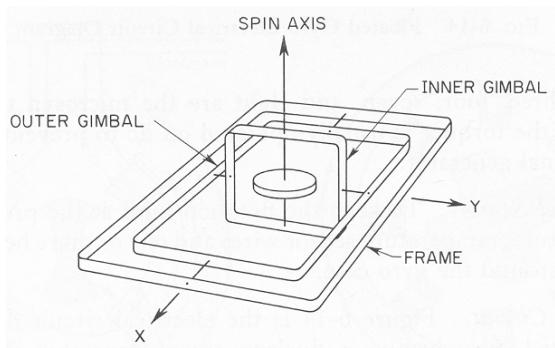


Figure 3 – TDF gyro schematics (after [4]).

A turning rate, ω about the IA causes a torque, T , along the OA, and vice versa. The IA is the axis around which a turning rate or an angle is measured and is the stable reference axis that the gyro provides for the inertial navigation system.

Two other very important gyro types that can be considered mechanical in nature are the hemispherical resonator gyro (HRG) and the dynamically tuned gyro (DTG). The first is a high performance vibratory gyro whose inertially sensitive element is fused silica [5] hemispherical shell with metal-coated rims. The HRG primary functional components (Fig. 4) include hemispherical resonator, the forcer and the

pick-off. They are bonded and contained within a sealed vacuum housing. A standing resonant wave on the shell's rim is electrostatically induced by the forcer. When the shell is rotated about the input axis (its symmetry axis), a standing wave pattern location precesses with respect to the fixed location on the body by a factor of 0.3. Capacitive pick-offs will detect a change in the location of nodes and anti-nodes in standing wave as gyro is rotated about its input axis.

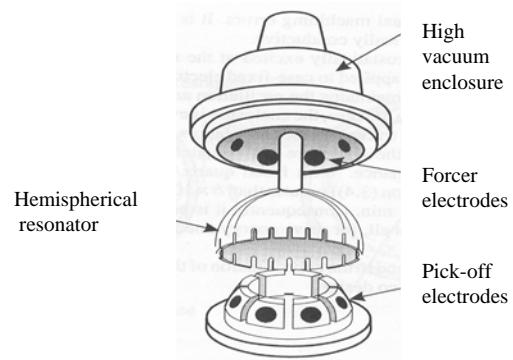


Figure 4 – HRG principle of operation (after [6]).

The basic idea behind DTG is reflected in Fig. 5. The gyro rotor is coupled to the spin motor shaft by a flexible Cardan type flexure joint creating a two-axis gimbal system.

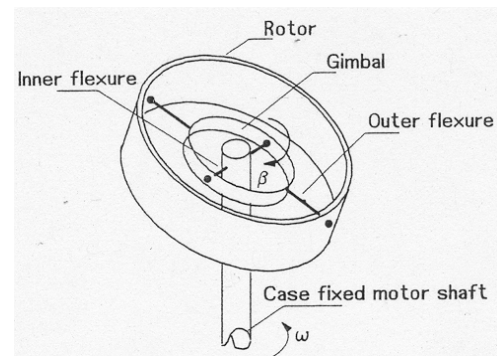


Figure 5 – DTG principle of operation (after [7]).

The flexural pivots have a torsional spring rate characteristics so they will exert a torque on a rotor when there is an angular displacement between the normal to the plane of the rotor and spin motor axis. This negative and restoring spring rate can be cancelled at a particular rotor speed by a dynamically created positive spring rate that appears from the torques exerted on the gimbals when there is an angular displacement of the rotor plane [8]. Once zero torques about gimbal axes are developed, the DTG behaves as an ideal free gyro with the rotor plane maintaining a fixed orientation in space.

DTG realization is given in Fig. 6. A motor keeps an iron rotor on bearings spinning at a fixed rate [9]. The appearance of outside input angular rotation results in a rotor precession that changes magnetic field at a signal generator.

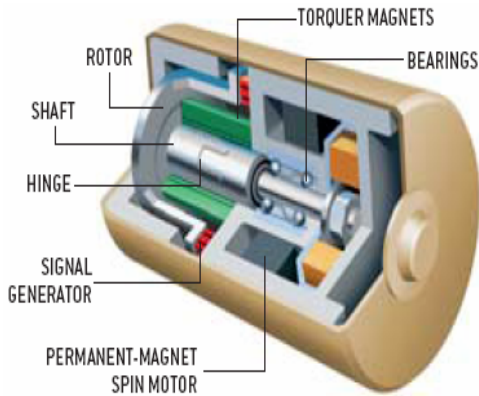


Figure 6 – DTG implementation (after [9]).

The generator then commands the torquer magnets (Fig. 7) to counteract the precession. One potential drawback of DTG design is its susceptibility to disturbances and oscillations at the tuned frequency and harmonics of this frequency.

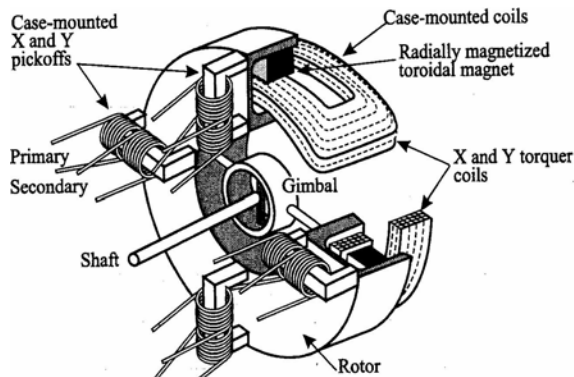


Figure 7 – DTG pick-offs and torquers (after [6]).

Thus, for reliable performance in a harsh environment, the alignment and mounting are the critical factors.

3. OPTICAL GYROS

Optical gyro class (Fig. 8) is presented by the ring laser gyros (RLG) and fiber-optic gyros (FOG). There is no spinning proof mass involved. Instead light is used as the sensing element. That has the advantage [7] to be unaffected by the dynamics of gyro environment.

On the other hand, the optical gyros can not be torqued or commanded like mechanical gyros [10]. Optical gyros

measure angular rate of rotation by sensing the resulting difference in the transit times for laser light waves traveling within a resonant cavity around a closed optical path length, L in opposite directions

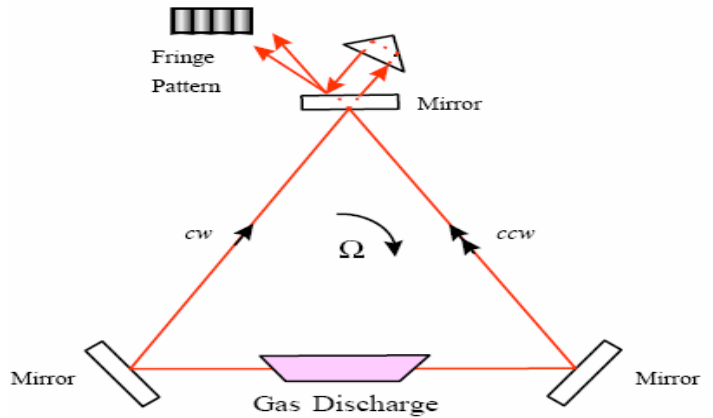


Figure 8 – RLG: principle of operation (after [9]).

At zero input rotation rate, the cw and ccw path lengths (Fig. 8) are equal and $\Delta L=0$. When RLG is rotated at rate Ω about an axis normal to the plane of the closed optical path, a difference in the path lengths is created ($\Delta L \sim \Omega$).

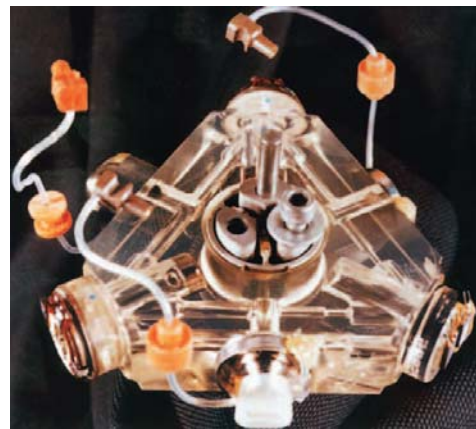


Figure 9 – RLG implementation (after [9]).

It produces [9] a frequency difference, Δv between the two waves that can be detected as a fringe pattern moves relative to the read-out photodiodes, $\Delta L/L = \Delta v/v$. As a result, $\Delta v \sim \Omega$ and direct digital output of the input angular rotation will be supplied by RLG operating (Fig. 9) as RIG.

Angular motion can also be sensed by detecting the phase difference between the two laser beams traveling in opposite directions (Fig. 10) as was implemented in FOG design.

Without rotation, transit time is the same for both waves at the detector and a perfect constructive interference occurs with a corresponding fringe pattern. Once input rotation

rate is introduced, it results in the arrival time difference between

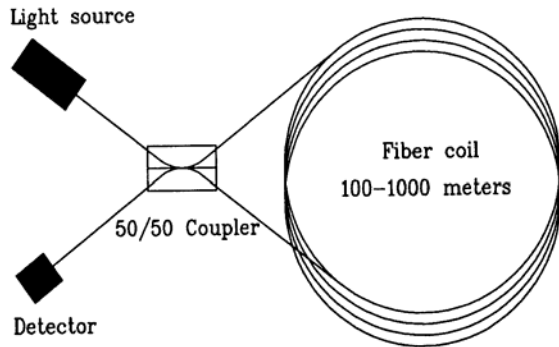


Figure 10 – FOG schematics (after [10]).

clock-wise and counter clock-wise beams after they passed through the fiber coil. This time difference (Sagnac effect) is proportional to the input rotation rate [11] and manifest itself as a phase shift causing a reduction in the intensity of



Figure 11 – FOG integration within LN-200 IMU.

light at the detector. As an example, a FOG-based IMU realization (Fig. 11) is shown above.

4. MEMS GYROS

The trend to lower the cost, size, and weight of inertial sensors opens a new window of opportunities to maintain current gyros performance with MEMS technology. To sense inertial angular motions, MEMS gyros rely on the detection of the Coriolis force acting on mass that undergoes linear vibrations in a rotating reference frame. Current MEMS gyros can be categorized either as simple oscillators; balance oscillators (tuning fork gyros) or shell resonators (wine glass, cylinder and vibrating ring gyros). Micromachining can shrink the sensor size by orders of magnitude, reduce the fabrication cost significantly, and allow the electronics to be integrated on the same silicon

chip [12].

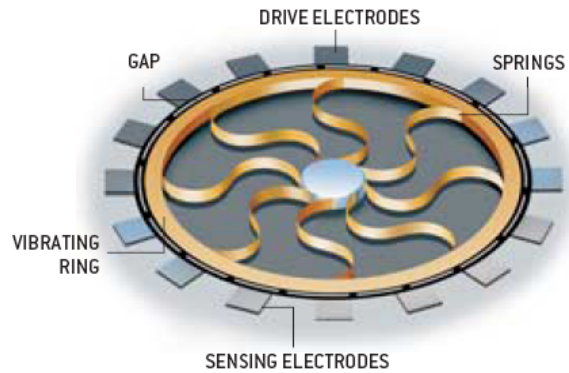


Figure 12 – Vibrating ring MEMS gyro structure (after [9]).

In a silicon vibrating gyro (Fig. 13), a ring is suspended by free floating, curved support springs attached to a central fixed post [9]. A standing vibration pattern is created by the drive electrodes (Fig. 12) electrostatically.

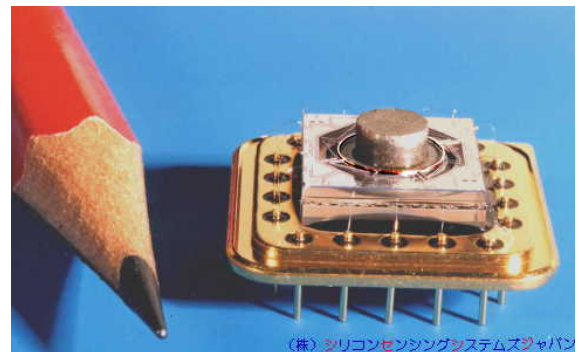


Figure 13 – Vibrating ring MEMS gyro implementation (after [13]).

When external rotation about input axis is applied to the ring, sensing electrodes determine its direction by monitoring the pattern. The amplitude of the distortion will indicate the rate of angular rotation.

Typical performance data for MEMS tuning fork gyros (Table 1) show technology status and expectations.

5. GYRO PERFORMANCE CHARACTERISTICS

There is a wide spectrum of parameters that characterize gyro performance. Among them [6] are common: operating

Table 1 – Performance figures of MEMS tuning fork gyros (after [14]).

life, MTBF; activation time; maximum rate; hysteresis; scale factor stability and non-linearity; cross-coupling; threshold,

* In many cases, the values given could be improved

Parameters	Current Sensors	Goals	Comments
Operating range, %s	100 ÷ 6000	100 ÷ 6000	Selectable
Turn-on bias stability, °/h	10 ÷ 150	< 1	All environments
In-run bias stability, °/h	3 ÷ 30	< 1	- 40 to 85 °C
Angle random walk (ARW), °/√h	0.01 ÷ 0.3	0.01 ÷ 0.03	Lower ARW at lower input rates
Turn-on scale factor stability, ppm	500 ÷ 1500	< 100	All environments
In-run scale factor stability, ppm	300 ÷ 1500	< 100	- 40 to 85 °C

resolution, bias stability, noise-spectrum; g-sensitivity; bandwidth; power consumption, etc. In order to choose right sensor for the mission, different environment factors - temperature extremes, shock level and duration, vibration level, ionizing radiation, etc. – and their impact on the gyro sensing element need to be considered as well.

For the mid-range applications with very high scale factor stability requirements, the RLG is the sensor choice [14]. It is also expected to see continuous MEMS gyro accuracy improvements.

Mechanical gyros provide lower short-term noise than optical gyros (but worse long-term stability), they have inertial memory [6], and they can offer longer life. Optical gyros, on the other hand, have no g-sensitivity, can measure

Principles of operation of major gyro technologies have already been described above. As a figure of merit, Table 2

Table 2 – Gyro typical performance characteristics* (after [14]).

summarizes some of the gyro specifications. Because bias

Characteristic	RIG	DTG	Flex gyroscope	DART/MHD	Vibratory gyro	RLG	FOG
g-Independent bias (°/h)	0.05–10	0.05–10	1–50	360–1800	360–1800	0.001–10	0.5–50
g-Dependent bias (°/h/g)	1–10	0.01–10	1–10	180	36–180	0	<1
Anisoelastic bias (°/h/g ²)	1–2	0.1–0.5	0.05–0.25	18–40	18	0	<0.1
Scale-factor non-linearity (%)	0.01–0.1	0.01–0.1	0.01–0.1	0.5–0.1	0.2–0.3	5–100	0.05–0.5
Bandwidth (Hz)	60	100	100	100/80	500	>200	>100
Maximum input rate (°/s)	>400	1000	>500	800/400	>1000	>1000	>1000
Shock resistance	Moderate	Moderate	Moderate	Moderate	>25 000g	Good	Good

and scale factor stability parameters in mechanical systems applications, respectively [14]. Despite advances in optical sensors, the high performance applications (1e-4 ÷

are better drift

tors, the most significant gyro ability are the

other major sources of concern.

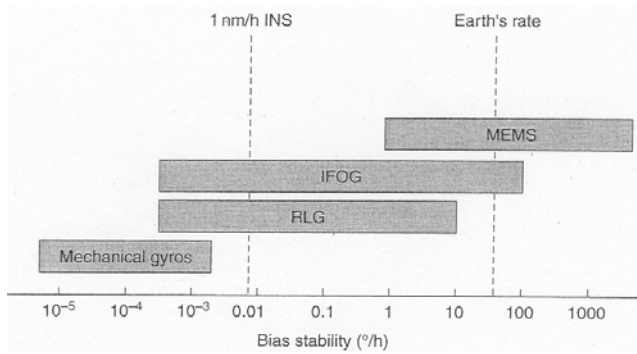


Figure 14 – Near-term gyro performance summary (after [14]).

To address those important issues, a rigorous technology comparison (Tables 2 and 3) makes mechanical gyros an alternative sensor technology (for this mission) that might be able to compete [15] with optical class gyros, RLG, and FOGs. Solid state technology implementation in the interfe-

rometric fiber-optic gyro (IFOG) design [6] practically removes lifetime constraint, but fiber darkening under radiation will seriously degrade sensor performance. The RLG has a lifetime limited by the helium leakage. They also [6] suffer under radiation (short term) from superradiance in the

Table 3 – Technology comparison: RLG, FOG and HRG (after [15]).

Category	Ring Laser Gyro (RLG)	Fiber Optic Gyro (FOG)	Hemispherical Resonator Gyro (HRG)
Phenomena	Electromagnetic wave properties Velocity = 3×10^8 m/s	Electromagnetic wave properties Velocity = 3×10^8 m/s	Stress wave properties Velocity = 6×10^3 m/s
Solid State Characteristics	Large stresses induced by dither mechanisms. Stress on mirrors for cavity control.	Hoop stress on fiber coil. Stress on integrated optic modulator.	Small stress due to stress wave pattern.
	Power in cavity	Power in thermoelectrical cooler of light source and light source	Microwatts applied to resonator to sustain stress wave
Gyro Construction	Machined quartz, sealed He/Ne cavity.	Precision-wound coil, spliced with multiple electrooptic components.	Machined metal resonator. Batch-produced pickoff/forcer assembly.
Gyro Economics	<ul style="list-style-type: none"> • Plasma control • Dither or bias control • Cavity Control • Photo detector Slow-speed electronics	<ul style="list-style-type: none"> • Source control • Thermoelectric cooler • Phase modulator control • Photodetector readout Fast electronics. 1-microsecond light transit time.	<ul style="list-style-type: none"> • Resonator control • Capacitive readout Slow speed electronics. 250-microsecond stress cycle time.
Memory Time Constant	None, if light source extinguished.	None, if light source extinguished.	Angular motion stored during power interrupts.
Size	3-axis; approximately 10 cu. in.	3-axis; approximately 16 cu. in.	3-axis; approximately 4 cu. in.
Performance			
• Bias	1 deg/h	1 deg/h	1 deg/h
• Random Walk	0.02	0.02	0.01
• Scale Factor	50 ppm	30-100 ppm	50-100 ppm
• Reaction Time	1s	1s	1s
Reliability/Life	Limited by He leakage out of small cavity.	Limited by lifetime of source and stressing of coil.	Limited by vacuum decay. Estimated life: 20 years (160,000 hours)

ionizing

radiation. Current DTG and HRG have similar performance characteristics (Table 4). Further evaluation in terms of reliability will suggest HRG since its operating life is expected to be longer (not depending on bearings and a lubricant). HRG sensing element, made of fused quartz, is inherently radiation hard. Thus, limited only by the electronics and vacuum decay, expected sensor lifetime is 20 years (Table 3)

HRG is a very high-Q ($\sim 10^7$) device with inertial memory so that vibrations of the shell will persist for several minutes [5] after power interruption. Optical gyros do not have such ability; once the power is off, they lose the reference.

HRG-based inertial measuring unit (IMU) has a successful flight history as well. It has been used on the Near Earth Asteroid Rendezvous (NEAR) spacecraft and on the Cassini mission which is still underway since October 1997. It is quite remarkable that HRG-based IMU was also a choice for JPL Europa Orbiter mission study [16].

6. HRG

Several critical performance characteristics such as noise, scale factor stability and bias stability of HRG-based IMU were tested (Table 4) and concluded to satisfy the Cassini mission key requirements.

Europa Orbiter study has been focused on identifying and mitigating the risk in surviving and operating the IMU in a harsh Jovian radiation environment. The effort involved the assessment of Litton's heritage space inertial reference unit (SIRU) product (Fig. 15) and needed changes to it to meet a broad set of Europa requirements [16]. Due to the advantages of HRG technology, results of the analysis have indicated that improved performance of Scalable SIRU has made it the baseline for the Europa IMU.

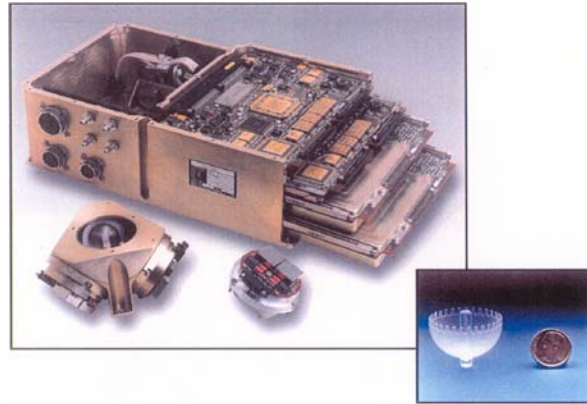


Figure 15 – HRG-based SIRUcore assembly (Litton, 1998).

The typical HRG readout and control electronics consists of analog signal conditioning circuits, an analog to digital interface, and a digital signal processor [18]. A simplified diagram of the readout and control mechanization (Fig. 16) includes four loops: (1) the phase lock loop to track the natural resonant frequency; (2) the amplitude control loop for sustaining and controlling the nominal resonator flex amplitude; (3) the quadrature control loop to correct for small unbalances on the resonator; and (4) the rate loop to apply a “rebalance” torque to hold the vibration pattern nodal position stationary [18].

Since then gyro performance parameters have been significantly improved. Current HRG-based IMUs can deliver bias stability in the region of $0.01^\circ/\text{h}$, low ARW of $0.0008\%/\sqrt{\text{h}}$ (3σ), angular white noise (AWN) of $0.003 \text{ arc-sec}/\sqrt{\text{Hz}}$ and excellent scale factor accuracy, with less than 1 ppm uncertainty [14].

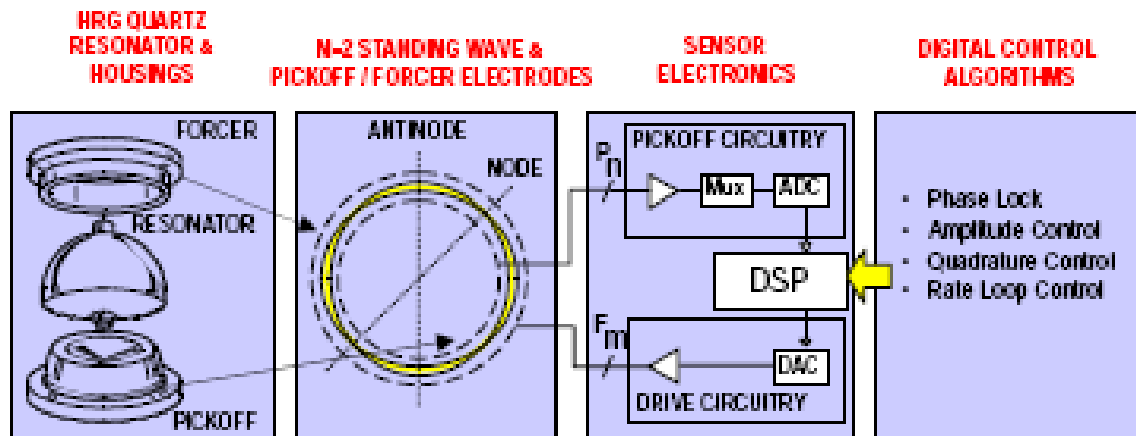


Figure 16 – Basic HRG functionality, readout and control (after [18]).

7. GYRO VENDORS

Gyro sensor manufacturers are presented (Table 4) by the following US – Crossbow [19], Honeywell [20], Kearfott [21], Northrop Grumman [22] and Japanese – Silicon Sensing Systems [13] vendors.

The solid state HRG uniquely offers the benefits of small size, extremely long life, and ultrahigh reliability for spacecraft pointing and control applications [17] and reasonably can be considered as a valid contender for the mission to Jupiter. Although a next generation system has not yet been identified [23], inertial sensor development is anticipated to concentrate on IFOG and HRG technology.

Table 4 – Major gyro vendors

Company	Model	Mass, kg	Power, W	Drift, °/hr	Max Rate, °/sec	ARW, °/√hr	Heritage
Crossbow	IMU700CA FOG-based	< 1.6	< 8	< 20	200	< 0.4	Avionics
Honeywell	HG1700 IMU RLG-based	< 1	< 8	2	1000	0.125±0.3	Tactical grade
Honeywell	MIMU	≤ 4.7	≤ 32	0.005	375	0.005	GEO, LEO
Honeywell	GG1320	< 0.5	0.375 or 1.6	0.0035	Not specified	0.0035	N/A
Kearfott	Gyroflex Mod II E/S	4.5	17	0.0015	15	0.0002	Voyager, Galileo
BEI	Gyrochip	0.05	0.75	< 0.05	1000	N/A	None
Northrop	LN-100S	10.4	30	0.003	N/A	0.0007	Launch vehicles, SBIRS
Northrop	SIRU	< 5	20	< 0.001	300	< 0.0001	NEAR, Cassini
Ferranti	125	0.43	1	0.002	100	Not specified	Spacelab, Miranda
Kearfott	TARA I, IRU	1.6	7.5	0.05	10	0.001	GSFC/MAP
Kearfott	TARA III, IRU	1.9	14±26	0.05	20	0.001	Earth observation
Northrop	LN-200	0.75	12	1	≤ 11,459	0.07±0.15	Clementine
Northrop	FOG 600	Not	specified	< 0.1	As Required	0.005	Inert. navigation
Northrop	FOG 1000	Not	specified	< 0.1	As Required	0.0035	Inert. navigation
Northrop	Scalable SIRU	4.54	20	0.003	12±300	0.0001	Deep Impact, Messenger, Herschel (2007)

8. SUMMARY

IMU reliability over 20 years of space mission is a serious concern. During maneuver and fault recovery operations as well as science data acquisition, IMU performance is quite important for spacecraft attitude stabilization and control.

Due to severe Jovian radiation environment, gyro survival and functionality have to be among the principal IMU characteristics contributing to the mission success.

REFERENCES

- [1] Charles D. Brown, Elements of Space Craft Design, AIAA Educational Series, 2002.
- [2] Spacecraft Attitude determination and Control, Ed. James R. Wertz, Kluwer Academic Publishers, 1978.
- [3] Vincent L. Pisacane, Fundamentals of Space Systems, 2nd Ed., Oxford University Press, 2005.

- [4] Inertial navigation, Principle of Guided Missile Design, Ed. G. Merrill, D. Van Nostrand Company, Inc., 1962.
- [5] Neil Barbour, "Inertial Components – Past, Present, and Future", AIAA2001-4290.
- [6] Antony Lawrence, Modern Inertial Technology, Springer, N.Y., 1998.
- [7] Shmuel Merhav, aerospace Sensor Systems and Applications, Springer, N.Y., 1996.
- [8] R.P.G. Collinson, Introduction to Avionics Systems, 2nd Ed., Kluwer Academic Publishers, 2003.
- [9] M. Fischetti, "Working Knowledge: Hidden Guides", Scientific American 286, 96, June 2002.
- [10] Christopher Jekeli, Inertial Navigation Systems with Geodetic Applications, W. de Gruyter, N.Y., 2001.
- [11] G. Sagnac, L'ether lumineux demontre par l'effet du vent relative d'ether dans un interferometer en rotation uniforme", C. R. Acad. Sci. 95, 708-710, 1913.
- [12] N. Yazdi et al., "Micromachined Inertial Sensors" Proc. IEEE 86, 1640-1659, 1998.
- [13] <http://www.spp.coo.jp/sssj/silicon-e.html>
- [14] D. H. Titterton, J. L. Weston, Strapdown Inertial Navigation Technology, 2nd Ed., Progress in Astronautics and Aeronautics, 207, 2004.
- [15] A. Matthews and F. J. Rybak, "Comparison of Hemispherical Resonator Gyro and Optical Gyros", IEEE AES Magazine, May 1992.
- [16] E. H. Konefat, E. C. Litty, S. K. Voigt, D. S. Wright, "Enabling Technology for NASA's Europa Orbiter Mission", AAS 01-001 107, 3-24, 2001.
- [17] E. Litty, L. Gresham, P. Toole, D. Beisecker, "Hemispherical Resonator Gyro: an IRU for Cassini", Proc. SPIE 2803, 299-310, 1996.
- [18] A. Matthews and D. A. Bauer, "The Hemispherical Resonator Gyro for precision pointing applications", Proc. SPIE 2466, 128-139, 1995.
- [19] <http://www.xbow.com>
- [20] <http://www.honeywell.com/sites/aero/Guidance-Navigation.htm>
- [21] <http://www.kearfoot.com>
- [22] <http://www.st.northropgrumman.com/capabilities/index.cfm#>
- [23] Neil Barbour and George Schmidt, "Inertial Sensor Technology Trends", IEEE Sensors Journal 1, 332-339, 2001.

ACKNOWLEDGMENT

The research described in this paper was carried out at the Jet Propulsion Laboratory, California Institute of Technology, under a contract with the National Aeronautics and Space Administration.

BIOGRAPHY

Sergei Jerebets received the M.S. Physics degree in 1997 from Washington State University (WA) and Ph.D. Physics degree in 2002 from Wesleyan University (CT). Sergei Jerebets has been with the Jet Propulsion Laboratory since then: first as a Caltech postdoctoral scholar and recently as a Member of the Technical Staff in the Precision Motion Control & Celestial Sensors group. His interests include ACS Sensors testing, calibration and development as well as image acquisition and analysis.



